EUROPEAN LABORATORY FOR PARTICLE PHYSICS (CERN)

CERN-EP/98-035
3rd March 1998

Measurement of the Fraction of Hadronic Z Decays into Charm Quark Pairs

The ALEPH Collaboration[1]

Abstract

The full statistics of hadronic Z decays collected with the ALEPH detector are analysed to measure, by three methods, the ratio, R_c, of the partial decay width of the Z into $c\bar{c}$ quarks to the total hadronic width. One method uses the inclusive p and $p_\perp$ spectra of electrons. The other two use a double-tagging technique to measure R_c independently of the charm-tagging efficiency. In one, the tagging procedure uses the reconstruction of high momentum charmed mesons (D^{*+}, D^+ and D^0) to detect the charm quarks. In the other, a charm quark is tagged from the D^*'s reconstructed in the $D^{*+} \to \pi^+ D^0$ decay channel and the other from the slow pion from the $D^{*-} \to \pi^- \bar{D}^0$ decay. The combination of these measurements leads to $R_c = \Gamma(Z \to c\bar{c})/\Gamma(Z \to \text{hadrons})) = 0.1681 \pm 0.0054(\text{stat}) \pm 0.0062(\text{syst})$.

(To be submitted to The European Physical Journal C)

[1]See next pages for the list of authors

The ALEPH Collaboration

R. Barate, D. Buskulic, D. Decamp, P. Ghez, C. Goy, J.-P. Lees, A. Lucotte, E. Merle, M.-N. Minard, J.-Y. Nief, B. Pietrzyk

Laboratoire de Physique des Particules (LAPP), IN^{2}P^3-CNRS, F-74019 Annecy-le-Vieux Cedex, France

R. Alemany, G. Boix, M.P. Casado, M. Chmeissani, J.M. Crespo, M. Delfino, E. Fernandez, M. Fernandez-Bosman, Ll. Garrido,[15] E. Graugès, A. Juste, M. Martinez, G. Merino, R. Miquel, Ll.M. Mir, I.C. Park, A. Pascual, J.A. Perlas, I. Riu, F. Sanchez

Institut de Física d'Altes Energies, Universitat Autònoma de Barcelona, E-08193 Bellaterra (Barcelona), Spain[7]

A. Colaleo, D. Creanza, M. de Palma, G. Gelao, G. Iaselli, G. Maggi, M. Maggi, S. Nuzzo, A. Ranieri, G. Raso, F. Ruggieri, G. Selvaggi, L. Silvestris, P. Tempesta, A. Tricomi,[3] G. Zito

Dipartimento di Fisica, INFN Sezione di Bari, I-70126 Bari, Italy

X. Huang, J. Lin, Q. Ouyang, T. Wang, Y. Xie, R. Xu, S. Xue, J. Zhang, L. Zhang, W. Zhao

Institute of High-Energy Physics, Academia Sinica, Beijing, The People's Republic of China[8]

D. Abbaneo, U. Becker, P. Bright-Thomas, D. Casper, M. Cattaneo, V. Ciulli, G. Dissertori, H. Drevermann, R.W. Forty, M. Frank, R. Hagelberg, J.B. Hansen, J. Harvey, P. Janot, B. Jost, I. Lehraus, P. Mato, A. Minten, L. Moneta,[21] A. Pacheco, J.-F. Pusztaszeri,[23] F. Ranjard, L. Rolandi, D. Rousseau, D. Schlatter, M. Schmitt,[25] O. Schneider, W. Tejessy, F. Teubert, I.R. Tomalin, H. Wachsmuth, A. Wagner[20]

European Laboratory for Particle Physics (CERN), CH-1211 Geneva 23, Switzerland

Z. Ajaltouni, F. Badaud, G. Chazelle, O. Deschamps, A. Falvard, C. Ferdi, P. Gay, C. Guicheney, P. Henrard, J. Jousset, B. Michel, S. Monteil, J-C. Montret, D. Pallin, P. Perret, F. Podlyski, J. Proriol, P. Rosnet

Laboratoire de Physique Corpusculaire, Université Blaise Pascal, IN^{2}P^3-CNRS, Clermont-Ferrand, F-63177 Aubière, France

J.D. Hansen, J.R. Hansen, P.H. Hansen, B.S. Nilsson, B. Rensch, A. Wäänänen

Niels Bohr Institute, DK-2100 Copenhagen, Denmark[9]

G. Daskalakis, A. Kyriakis, C. Markou, E. Simopoulou, I. Siotis, A. Vayaki

Nuclear Research Center Demokritos (NRCD), GR-15310 Attiki, Greece

A. Blondel, G. Bonneaud, J.-C. Brient, P. Bourdon, A. Rougé, M. Rumpf, A. Valassi,[6] M. Verderi, H. Videau

Laboratoire de Physique Nucléaire et des Hautes Energies, Ecole Polytechnique, IN^{2}P^3-CNRS, F-91128 Palaiseau Cedex, France

E. Focardi, G. Parrini, K. Zachariadou

Dipartimento di Fisica, Università di Firenze, INFN Sezione di Firenze, I-50125 Firenze, Italy

M. Corden, C. Georgiopoulos, D.E. Jaffe

Supercomputer Computations Research Institute, Florida State University, Tallahassee, FL 32306-4052, USA [13,14]

A. Antonelli, G. Bencivenni, G. Bologna,[4] F. Bossi, P. Campana, G. Capon, F. Cerutti, V. Chiarella, G. Felici, P. Laurelli, G. Mannocchi,[5] F. Murtas, G.P. Murtas, L. Passalacqua, M. Pepe-Altarelli

Laboratori Nazionali dell'INFN (LNF-INFN), I-00044 Frascati, Italy

L. Curtis, A.W. Halley, J.G. Lynch, P. Negus, V. O'Shea, C. Raine, J.M. Scarr, K. Smith, P. Teixeira-Dias, A.S. Thompson, E. Thomson

Department of Physics and Astronomy, University of Glasgow, Glasgow G12 8QQ,United Kingdom[10]

O. Buchmüller, S. Dhamotharan, C. Geweniger, G. Graefe, P. Hanke, G. Hansper, V. Hepp, E.E. Kluge, A. Putzer, J. Sommer, K. Tittel, S. Werner, M. Wunsch

Institut für Hochenergiephysik, Universität Heidelberg, D-69120 Heidelberg, Germany[16]

R. Beuselinck, D.M. Binnie, W. Cameron, P.J. Dornan,[2] M. Girone, S. Goodsir, E.B. Martin, N. Marinelli, A. Moutoussi, J. Nash, J.K. Sedgbeer, P. Spagnolo, M.D. Williams

Department of Physics, Imperial College, London SW7 2BZ, United Kingdom[10]

V.M. Ghete, P. Girtler, E. Kneringer, D. Kuhn, G. Rudolph

Institut für Experimentalphysik, Universität Innsbruck, A-6020 Innsbruck, Austria[18]

A.P. Betteridge, C.K. Bowdery, P.G. Buck, P. Colrain, G. Crawford, A.J. Finch, F. Foster, G. Hughes, R.W.L. Jones, M.I. Williams

Department of Physics, University of Lancaster, Lancaster LA1 4YB, United Kingdom[10]

I. Giehl, A.M. Greene, C. Hoffmann, K. Jakobs, K. Kleinknecht, G. Quast, B. Renk, E. Rohne, H.-G. Sander, P. van Gemmeren, C. Zeitnitz

Institut für Physik, Universität Mainz, D-55099 Mainz, Germany[16]

J.J. Aubert, C. Benchouk, A. Bonissent, G. Bujosa, J. Carr,[2] P. Coyle, F. Etienne, O. Leroy, F. Motsch, P. Payre, M. Talby, A. Sadouki, M. Thulasidas, K. Trabelsi

Centre de Physique des Particules, Faculté des Sciences de Luminy, IN^{2}P^3-CNRS, F-13288 Marseille, France

M. Aleppo, M. Antonelli, F. Ragusa

Dipartimento di Fisica, Università di Milano e INFN Sezione di Milano, I-20133 Milano, Italy

R. Berlich, W. Blum, V. Büscher, H. Dietl, G. Ganis, H. Kroha, G. Lütjens, C. Mannert, W. Männer, H.-G. Moser, S. Schael, R. Settles, H. Seywerd, H. Stenzel, W. Wiedenmann, G. Wolf

Max-Planck-Institut für Physik, Werner-Heisenberg-Institut, D-80805 München, Germany[16]

J. Boucrot, O. Callot, S. Chen, A. Cordier, M. Davier, L. Duflot, J.-F. Grivaz, Ph. Heusse, A. Höcker, A. Jacholkowska, D.W. Kim,[12] F. Le Diberder, J. Lefrançois, A.-M. Lutz, M.-H. Schune, E. Tournefier, J.-J. Veillet, I. Videau, D. Zerwas

Laboratoire de l'Accélérateur Linéaire, Université de Paris-Sud, IN^{2}P^3-CNRS, F-91405 Orsay Cedex, France

P. Azzurri, G. Bagliesi,[2] G. Batignani, S. Bettarini, T. Boccali, C. Bozzi, G. Calderini, M. Carpinelli, M.A. Ciocci, R. Dell'Orso, R. Fantechi, I. Ferrante, L. Foà,[1] F. Forti, A. Giassi, M.A. Giorgi, A. Gregorio, F. Ligabue, A. Lusiani, P.S. Marrocchesi, A. Messineo, F. Palla, G. Rizzo, G. Sanguinetti, A. Sciabà, R. Tenchini, G. Tonelli,[19] C. Vannini, A. Venturi, P.G. Verdini

Dipartimento di Fisica dell'Università, INFN Sezione di Pisa, e Scuola Normale Superiore, I-56010 Pisa, Italy

G.A. Blair, L.M. Bryant, J.T. Chambers, M.G. Green, T. Medcalf, P. Perrodo, J.A. Strong, J.H. von Wimmersperg-Toeller

Department of Physics, Royal Holloway & Bedford New College, University of London, Surrey TW20 OEX, United Kingdom[10]

D.R. Botterill, R.W. Clifft, T.R. Edgecock, S. Haywood, P.R. Norton, J.C. Thompson, A.E. Wright

Particle Physics Dept., Rutherford Appleton Laboratory, Chilton, Didcot, Oxon OX11 OQX, United Kingdom[10]

B. Bloch-Devaux, P. Colas, S. Emery, W. Kozanecki, E. Lançon,[2] M.-C. Lemaire, E. Locci, P. Perez, J. Rander, J.-F. Renardy, A. Roussarie, J.-P. Schuller, J. Schwindling, A. Trabelsi, B. Vallage

CEA, DAPNIA/Service de Physique des Particules, CE-Saclay, F-91191 Gif-sur-Yvette Cedex, France[17]

S.N. Black, J.H. Dann, R.P. Johnson, H.Y. Kim, N. Konstantinidis, A.M. Litke, M.A. McNeil, G. Taylor

Institute for Particle Physics, University of California at Santa Cruz, Santa Cruz, CA 95064, USA[22]

C.N. Booth, C.A.J. Brew, S. Cartwright, F. Combley, M.S. Kelly, M. Lehto, J. Reeve, L.F. Thompson

Department of Physics, University of Sheffield, Sheffield S3 7RH, United Kingdom[10]

K. Affholderbach, A. Böhrer, S. Brandt, G. Cowan, C. Grupen, P. Saraiva, L. Smolik, F. Stephan

Fachbereich Physik, Universität Siegen, D-57068 Siegen, Germany[16]

M. Apollonio, L. Bosisio, R. Della Marina, G. Giannini, B. Gobbo, G. Musolino

Dipartimento di Fisica, Università di Trieste e INFN Sezione di Trieste, I-34127 Trieste, Italy

J. Rothberg, S. Wasserbaech

Experimental Elementary Particle Physics, University of Washington, WA 98195 Seattle, U.S.A.

S.R. Armstrong, E. Charles, P. Elmer, D.P.S. Ferguson, Y. Gao, S. González, T.C. Greening, O.J. Hayes, H. Hu, S. Jin, P.A. McNamara III, J.M. Nachtman,[24] J. Nielsen, W. Orejudos, Y.B. Pan, Y. Saadi, I.J. Scott, J. Walsh, Sau Lan Wu, X. Wu, G. Zobernig

Department of Physics, University of Wisconsin, Madison, WI 53706, USA[11]

---

[1]Now at CERN, 1211 Geneva 23, Switzerland.

[2]Also at CERN, 1211 Geneva 23, Switzerland.

[3]Also at Dipartimento di Fisica, INFN, Sezione di Catania, Catania, Italy.

[4]Also Istituto di Fisica Generale, Università di Torino, Torino, Italy.

[5]Also Istituto di Cosmo-Geofisica del C.N.R., Torino, Italy.

[6]Supported by the Commission of the European Communities, contract ERBCHBICT941234.

[7]Supported by CICYT, Spain.

[8]Supported by the National Science Foundation of China.

[9]Supported by the Danish Natural Science Research Council.

[10]Supported by the UK Particle Physics and Astronomy Research Council.

[11]Supported by the US Department of Energy, grant DE-FG0295-ER40896.

[12]Permanent address: Kangnung National University, Kangnung, Korea.

[13]Supported by the US Department of Energy, contract DE-FG05-92ER40742.

[14]Supported by the US Department of Energy, contract DE-FC05-85ER250000.

[15]Permanent address: Universitat de Barcelona, 08208 Barcelona, Spain.

[16]Supported by the Bundesministerium für Bildung, Wissenschaft, Forschung und Technologie, Germany.

[17]Supported by the Direction des Sciences de la Matière, C.E.A.

[18]Supported by Fonds zur Förderung der wissenschaftlichen Forschung, Austria.

[19]Also at Istituto di Matematica e Fisica, Università di Sassari, Sassari, Italy.

[20]Now at Schweizerischer Bankverein, Basel, Switzerland.

[21]Now at University of Geneva, 1211 Geneva 4, Switzerland.

[22]Supported by the US Department of Energy, grant DE-FG03-92ER40689.

[23]Now at School of Operations Research and Industrial Engineering, Cornell University, Ithaca, NY 14853-3801, U.S.A.

[24]Now at University of California at Los Angeles (UCLA), Los Angeles, CA 90024, U.S.A.

[25]Now at Harvard University, Cambridge, MA 02138, U.S.A.

1 Introduction

The measurement of the ratio $R_c = \Gamma(Z \to c\bar{c})/\Gamma(Z \to \text{hadrons})$ provides an important test of the Standard Model because it is virtually independent of the value of top quark mass as well as of supersymmetric extensions of the Standard Model as the one-loop corrections to the propagator cancel in the ratio. The small residual dependence comes from the $b\bar{b}$ vertex in the denominator. A departure from the Standard Model prediction would therefore be a hint for exotic physics [1]. Experimentally the ratio of the partial widths, R_c, is measured from the ratio of the cross-sections, with a small correction due to the photon exchange diagram.

In this paper the results from three different measurements of R_c are presented. The full statistics collected by the ALEPH detector between 1991 and 1995 are used, about four millions hadronic Z decays, selected as described in Ref. [2].

The first analysis employs the measurement of the yield of hadronic events in which electrons are identified. The measurement relies on accurate studies of the electron identification performance including the main sources of non-prompt electrons which are converted photons and misidentified hadrons. The kinematic distributions of the electrons allow the discrimination of the different contributions to the selected sample. The b contribution is measured directly with data by means of a double-tagging technique. This analysis is then limited by both the knowledge of the semileptonic c branching ratio and the modelling of the $c \to e$ spectrum.

The two other analyses rely on double-tagging techniques to measure R_c independently of the charm-tagging efficiency. They both use high momentum charmed mesons to identify the two quarks from a $Z \to c\bar{c}$ decay. The $Z \to b\bar{b}$ contribution to the selected D sample is measured with data by exploiting the long lifetime and high mass of b hadrons. In the first of these methods, the exclusive reconstruction of charmed meson D^{*+}, D^+ and D^0 decays[1] allows a D meson tag to be performed on a hemisphere basis. The second method benefits from the high efficiency of an inclusive D^{*+} selection. The small Q value of the decay $D^{*+} \to \pi^+ D^0$ allows the identification of the D^{*+} by requiring a slow pion at low transverse momentum with respect to the D^{*+} line of flight, which is measured by the direction of the jet to which the pion belongs. This slow pion tag is used as a second tag once a D^{*-} is reconstructed in the opposite hemisphere.

2 The ALEPH detector

A detailed description of the ALEPH detector and its performance can be found in Refs. [3] and [4]. Only a brief review is given here.

Charged particles are detected in the central part of the detector, consisting of a two-layer silicon vertex detector (VDET) with double-sided (r-ϕ and z) readout, a cylindrical drift chamber and a large time projection chamber (TPC), which together measure up to 33 coordinates along the charged particle trajectories. Tracking is performed in a 1.5 T magnetic field provided by a superconducting solenoid. The combined system yields a transverse momentum resolution of $\Delta p_\perp/p_\perp = 6 \times 10^{-4} p_\perp \oplus 0.005$ ($p_\perp$ in GeV/c) and the impact parameter resolution is $25 \oplus 95/p\,\mu$m (p in GeV/c) in both the

[1] Charge conjugation implied throughout

r-ϕ and z views. The TPC also provides up to 338 measurements of ionization (dE/dx) allowing particle identification.

The electromagnetic calorimeter is a lead/wire-chamber sandwich operated in proportional mode. It is read out in projective towers of typically 15×15 mrad^2 size segmented in three longitudinal sections. It is used together with dE/dx measurements in the TPC to identify electrons. The iron return yoke is instrumented with streamer tubes to provide a measurement of the hadronic energy and, together with external chambers, of muon identification.

3 Measurement of R_c from Inclusive Electrons

This analysis relies heavily on the identification of low momentum leptons. Muon candidates were not considered since in the low momentum region the background contamination is high compared to that for electrons.

3.1 Data Analysis

Electrons are identified in hadronic events according to the criteria described in [5], with the momentum cut lowered to 2 GeV/c. Only events with $|\cos\theta_{\rm thrust}| \leq 0.7$ are considered, which corresponds to the VDET acceptance. The selection of hadronic events and the acceptance cut induce, according to the Monte-Carlo simulation, a $(0.1 \pm 0.1)\%$ bias in favour of $c\bar{c}$ events, which is corrected for when measuring R_c. A sample of 168887 electron candidates is selected from 3.7 million hadronic events. Candidates come from b and c semileptonic decays, cascade decays b $\rightarrow$ c $\rightarrow$ e, τ and Ψ decays, non prompt-electron sources and misidentified hadrons. The momentum p and the transverse momentum $p_\perp$ of the electron candidates are used to separate the different contributions to the sample. The transverse momentum is defined with respect to the jet to which the electron candidate belongs. Best discrimination is achieved by calculating the jet axis after removing the selected electron candidate and by using both neutral and charged particles in the jet definition [5].

The density of selected electron candidates for each hadronic Z decay $\mathcal{P}(p,p_\perp)$ is expressed as

$$\mathcal{P}(p,p_\perp) = \mathrm{R_b}\mathcal{P}^{\mathrm{b}\rightsquigarrow\mathrm{e}}(p,p_\perp) + \mathrm{R_c}\mathcal{P}^{\mathrm{c}\rightarrow\mathrm{e}}(p,p_\perp) + (1-\mathrm{R_b})\mathcal{P}^{\mathrm{back}}_{\mathrm{udsc}}(p,p_\perp) \ ,$$

where $\mathcal{P}^{\mathrm{b}\rightsquigarrow\mathrm{e}}(p,p_\perp)$ is the density of electron candidates from all sources for each Z $\rightarrow$ b$\bar{\mathrm{b}}$ event, $\mathcal{P}^{\mathrm{c}\rightarrow\mathrm{e}}(p,p_\perp)$ is the density of prompt electrons for each Z $\rightarrow$ c$\bar{\mathrm{c}}$ event, $\mathcal{P}^{\mathrm{back}}_{\mathrm{udsc}}(p,p_\perp)$ is the density of background to prompt electron for each Z $\rightarrow$ q$\bar{\mathrm{q}}$ event, with q = u, d, s or c. Using the forms of these densities as determined in the following sections, $\mathrm{R_c}$ is obtained from a binned maximum likelihood fit to the $\mathcal{P}(p,p_\perp)$ distribution in the data.

3.2 Determination of $\mathcal{P}^{\mathrm{b}\rightsquigarrow\mathrm{e}}(p,p_\perp)$

The electron candidate density $\mathcal{P}^{\mathrm{b}\rightsquigarrow\mathrm{e}}(p,p_\perp)$ for the b component is measured directly on data, from a pure b$\bar{\mathrm{b}}$ sample, as in [6]. The events are divided into hemispheres defined by the plane orthogonal to the thrust axis, and a cut on a lifetime tagging probability [7] is applied to obtain a sample of hemispheres enriched in b events, $N^{\mathrm{tag}}_{\mathrm{hemi}}$.

The cut used results in a selection efficiency for the identification of $Z \to b\bar{b}$ events with $|\cos\theta_{\rm thrust}| \leq 0.7$ of 25% [7] and a purity, $P^{\rm b}_{\rm hemi}$, greater than 96%. Electron candidates are searched for in the hemisphere opposite to the tagged one. After this requirement the purity, $P^{\rm b}_{\rm e}(p, p_\perp)$, is greater than 98 %. The $(p, p_\perp)$ spectrum is measured to give $N^{\rm tag}_{\rm e}(p, p_\perp)$.

The b density, $\mathcal{P}^{\rm b\rightsquigarrow e}(p, p_\perp)$, is given by the formula :

$$\mathcal{P}^{\rm b\rightsquigarrow e}(p, p_\perp) = (1 + \rho(p, p_\perp)) \times \frac{N^{\rm tag}_{\rm e}(p, p_\perp) P^{\rm b}_{\rm e}(p, p_\perp)}{N^{\rm tag}_{\rm hemi} P^{\rm b}_{\rm hemi}}$$

The $\rho(p, p_\perp)$ parameter corrects for any bias which may be introduced as a result of the cut on the lifetime tagging probability in the opposite hemisphere. This and other uncertainties, such as those arising from udsc contamination of the b electron candidate sample are investigated in section 3.5.

The normalization of the b content in the overall selected electron candidate sample is governed by R_b. In the fit the absolute normalization of the b contribution has been left free, since the b electron candidate spectrum is very well determined and well separated kinematically from the other flavours. Hence this R_c measurement does not depend on R_b.

3.3 Determination of $\mathcal{P}^{\rm c\to e}(p, p_\perp)$

The density $\mathcal{P}^{\rm c\to e}(p, p_\perp)$ is not directly measured from ALEPH data. It can be rewritten in the following form:

$$\mathcal{P}^{\rm c\to e}(p, p_\perp) = \mathcal{B}({\rm c} \to {\rm e}) \mathcal{F}^{\rm c\to e}(p, p_\perp) \epsilon(p, p_\perp),$$

where $\epsilon(p, p_\perp)$ is the efficiency, obtained from data [4, 5], to detect and identify an electron, and $\mathcal{F}^{\rm c\to e}(p, p_\perp)$ is the normalized spectrum of electrons coming from the semileptonic decay of a primary charmed hadron. Two processes determine $\mathcal{F}^{\rm c\to e}(p, p_\perp)$: c-quark fragmentation and charmed hadron semileptonic decays. The functional form of the c-quark fragmentation in the Monte Carlo is taken from [8] with the mean fractional energy of the c hadron $\langle X_{\rm c} \rangle \equiv E_{\rm had}/E_{\rm beam}$ as a free parameter. For the charm semileptonic decay spectrum Monte Carlo events are re-weighted to reproduce the average spectrum measured by DELCO and MARK III [9].

For the semileptonic branching ratio $\mathcal{B}({\rm c} \to {\rm e})$ the average of measurements from lower energy experiments, $\mathcal{B}({\rm c} \to {\rm e}) = 0.098 \pm 0.005$ [9], is used.

3.4 Determination of $\mathcal{P}^{\rm back}_{\rm udsc}(p, p_\perp)$

Two main processes contribute to this last component: electrons from converted photons or Dalitz π^0 decays (in which only one electron of the pair is identified) and hadrons faking electrons. These two backgrounds have been studied directly in the data as a function of p and $p_\perp$ [4, 5].

The contamination of hadrons faking electrons is determined from a comparison of the dE/dx and calorimeter information. The p and $p_\perp$ distributions of electrons from converted photons are measured, in $q\bar{q}$ events, when both electrons of the pair are identified. By comparison with an equivalent Monte Carlo sample, correction factors are obtained and applied to photon conversions with only one identified electron. As

electrons from converted photons or Dalitz π^0 decays constitute the main background to the c $\rightarrow$ e process, their absolute normalization is also fitted to the data.

A residual background, determined from the Monte-Carlo, is due to the decays of light hadrons. A small background component originating from semileptonic decays of heavy flavour produced in gluon splitting is also included in $\mathcal{P}^{\rm back}_{\rm udsc}(p, p_\perp)$. More details on the gluon splitting rate are given in section 4.1.4.

3.5 Systematics

3.5.1 $\mathcal{P}^{\rm b\rightsquigarrow e}(p, p_\perp)$ systematics

The cut on the lifetime tagging probability biases the lepton spectra because of momentum and geometrical correlations between hemispheres. While knowledge of the total correlation is not relevant - since it is part of the fitted b normalization - the distortion of the $(p, p_\perp)$ spectrum due to the variation of the correlation $\rho(p, p_\perp)$ must be investigated.

Figure 1 (a) and (b) shows the ratio of the spectra -biased and unbiased- measured in a full Monte Carlo simulation for three values of the lifetime tagging probability as a function of the transverse momentum and momentum of electrons. Within the statistical error, no significant bias is observed at the $P_H^{\rm cut}$ value used in the analysis (10^{-4}). The statistical accuracy of this test is used to assign a systematic error. Distortions due to the B hadron momentum correlations were found to be negligible (effect on $R_c < 0.0001$). Additionally, an attempt was made to extract information on the distortion from data. A soft cut on the lifetime tagging probability was applied in one hemisphere in order to have a pure ($\approx 80\%$) and less biased sample of b - the non b background component has been subtracted by making use of the Monte Carlo predictions. The electron spectra in the opposite hemisphere were then compared to the spectra of the reference sample. Again, no significant discrepancy is observed and the statistical power of the test is used to assign an additional systematic error. These errors are referred to as "correlations" in Table 1.

An additional systematic error is caused by the contamination of the b electron sample by udsc events. This depends on $(p, p_\perp)$ but is always less than 2%. The resulting systematic error is dominated by charm. It is determined as in [7] and is denoted "b tagging" in Table 1.

3.5.2 $\mathcal{P}^{\rm c\rightarrow e}(p, p_\perp)$ systematics

Four sources of uncertainties, in addition to the uncertainties on the $\mathcal{B}$(c $\rightarrow$ e) quantity, have been studied for the $c \rightarrow e$ process. In decreasing order of importance they are:

- The modelling uncertainty is studied by varying, within their errors, the parameters of the ACCMM model [10] of the c-hadron semileptonic decay fitted to the DELCO and MARK III data. The prescription used is that of the LEP Electroweak Working Group [9] and the resulting error is referred as "c decay modelling" in Table 1.

- The electron identification efficiency is measured directly from the data as a function of (p,$p_\perp$) with an accuracy of 1.5 %, following the method of [4, 5].

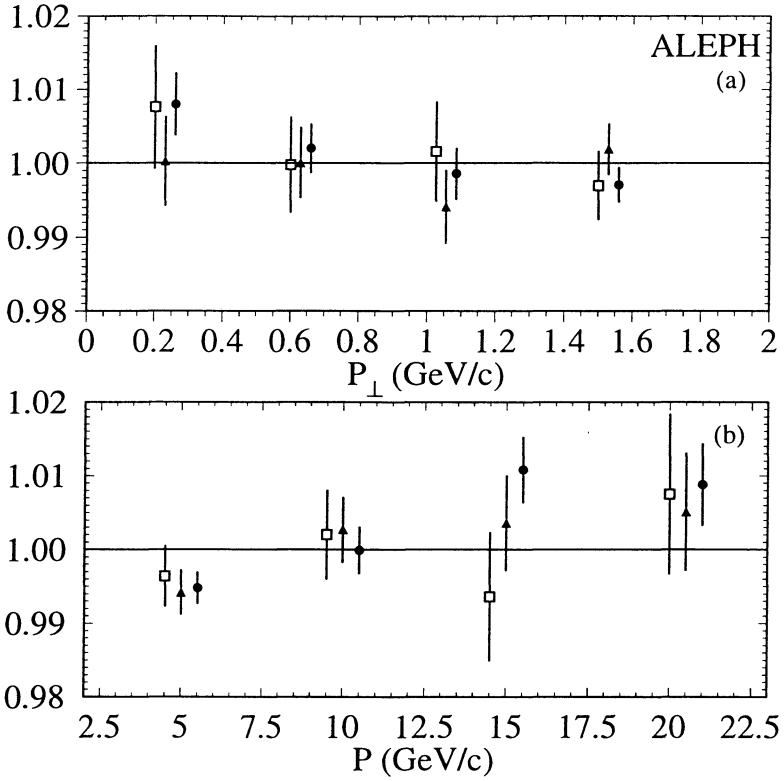

Figure 1: *Ratio of the spectra of the electron candidates, biased / unbiased, as a function of the transverse momentum (a) and momentum of electrons (b), measured in a full Monte Carlo simulation for three cut values of the lifetime tagging probability* $P_H^{\rm cut} = 10^{-2}, 10^{-3}, 10^{-4}$ *denoted respectively by dots, triangles and white squares. The latter represent the value used in the analysis.*

- A third source of uncertainty concerns the simulation of the fragmentation tracks in the jet containing the electron, which contribute to build up the jet axis with the tracks coming from the c-hadron decay. It has been studied by selecting fast D* as in Ref. [11]. The angle between the D* and the jet is measured from the data and compared with Monte Carlo expectation. The comparison provides an estimate of the associated error and is referred to as "jet modelling" in Table 1.

- Although the c-hadron mean energy is measured simultaneously with R_c, the choice of the Peterson fragmentation scheme introduces a systematic uncertainty, which has been estimated by performing the measurement with two alternative fragmentation models (Collins [12] and Kartvelishvili [13]). The error is referred to as "fragmentation modelling" in Table 1.

3.5.3 $\mathcal{P}_{\rm udsc}^{\rm back}(p, p_\perp)$ systematics

Two types of systematic uncertainties can be distinguished: the knowledge of the total amount of background - here only the number of hadrons faking electrons is

Table 1: *List of the errors on the measurement of* R_c.

Source	ΔR_c
correlations	± 0.0009
b tagging	± 0.0002
c decay modelling	± 0.0039
electron ID efficiency	± 0.0023
jet modelling	± 0.0014
fragmentation modelling	± 0.0013
misidentified hadrons	± 0.0022
misidentified hadrons shape	± 0.0020
electron conversion shape	± 0.0013
gluon splitting	± 0.0004
$\mathcal{B}(c \to e)$	± 0.0084
TOTAL stat	± 0.0062

considered since the number of electrons from converted photons is fitted - and the knowledge of the shape of its $(p, p_\perp)$ distribution. For each type of background, the data are used to measure the $(p, p_\perp)$ distributions and the statistical precision of these measurements gives one part of the error. Another part comes from the fact that the $(p, p_\perp)$ distributions are measured when all types of quarks are produced while only u, d, s or c quarks are considered for $\mathcal{P}^{\text{back}}_{\text{udsc}}(p, p_\perp)$. Consequently the shapes of the $(p, p_\perp)$ distributions are specifically studied in a b-enriched sample selected as described in section 3.2. They are found to be the same within the statistical errors. These statistical errors are taken as systematics. These errors are referred to as "electron background shape" and "electron conversion shape" in Table 1.

3.6 Results

The normalization of the b and non-prompt electron components, as well as $\langle X_c \rangle$ are measured simultaneously with R_c by fitting the $(p, p_\perp)$ distributions to the data. The statistical errors on the determination of the shape of the b component and the non-prompt electron background are included in the fit. The following result is found:

$$R_c \mathcal{B}(c \to e) = 0.01645 \pm 0.00061(\text{stat.}) \pm 0.00059(\text{syst.}) \ ,$$

leading to

$$R_c = 0.1675 \pm 0.0062(\text{stat.}) \pm 0.0060(\text{syst.}) \pm 0.0084(\text{BR}) \ ,$$

where the last uncertainty comes from $\mathcal{B}(c \to e)$. A small correction of -3×10^{-4} is applied to this result, and throughout the rest of the paper, to subtract the photon exchange diagram contribution. The mean fraction of energy carried by the charmed hadron after fragmentation is found to be $\langle X_c \rangle = 0.504 \pm 0.010$, in good agreement with the previous ALEPH publications [14, 15] and the current world average [6]. The correlation between these two quantities is -0.33. The main systematic errors are summarised in Table 1. Figure 2 shows the fit result projected onto the p and $p_\perp$ axes, after the b component is subtracted, with $\chi^2/\text{dof} = 1.1$.

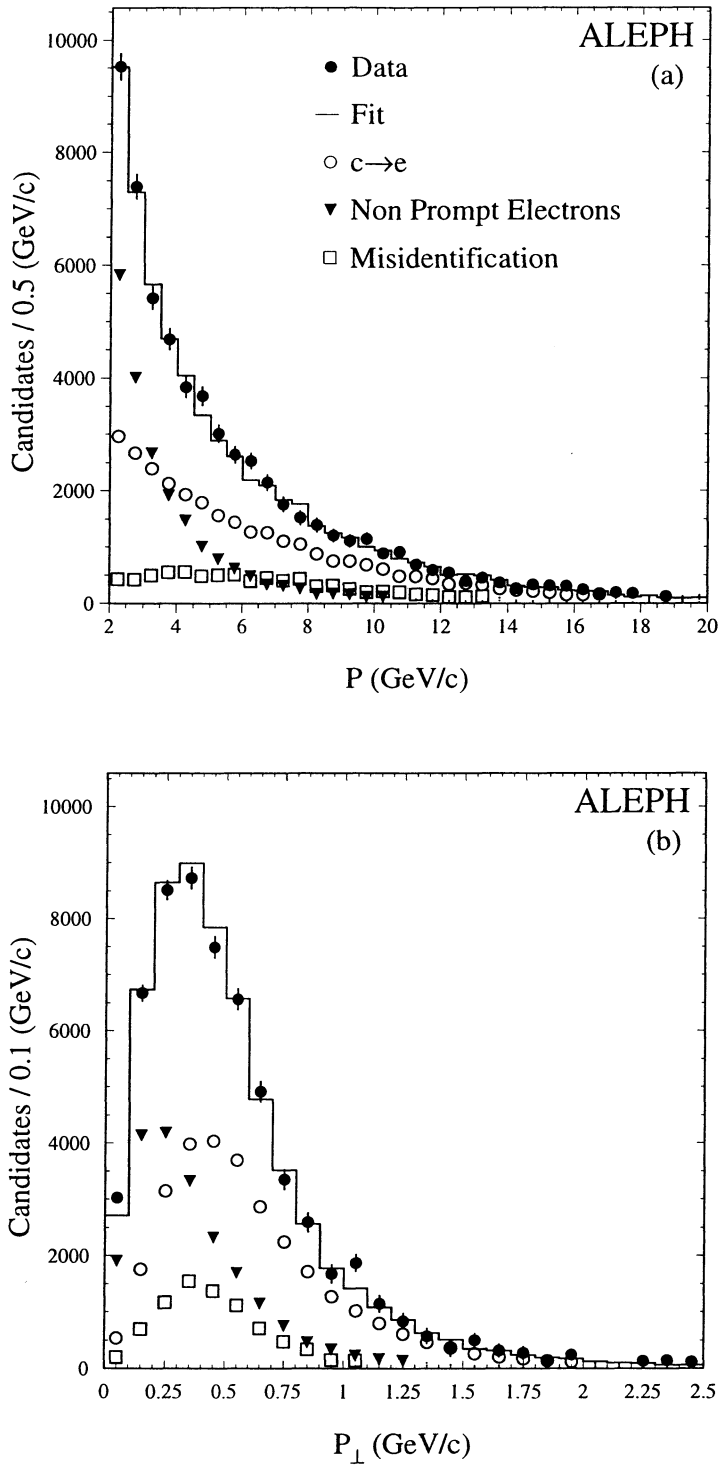

Figure 2: *Result of the fit to the single lepton sample, after subtraction of the* b *component (taken from data), as a function of p (a) and* $p_\perp$ *(b).*

Although still systematically limited, this new analysis has much improved the systematics with respect to the previous ALEPH measurements of R_c with leptons, performed on the data collected in 1990 and 1991 [14].

4 Measurement of R_c with a Double Charm-tagging Method

Two analyses relying on a double-tagging technique using D mesons as a signature of charm production are performed. The double-tagging technique offers the advantage of being independent of the tagging efficiency. Each event is divided into two hemispheres according to the plane orthogonal to thrust axis direction, determined using both charged tracks and neutral energy clusters reconstructed in the calorimeter. A D meson is then searched for in each hemisphere, either by full reconstruction in an exclusive decay mode or by an inclusive identification using the slow pion from the $D^{*+} \to D^0 \pi_s^+$ decay.

Charmed mesons are produced both from c and b quarks, the tagging efficiency ξ_q is

$$\xi_q = P(q \to D)\mathcal{B}_D \epsilon^{q \to D} ,$$

where $P(q \to D)$ is the probability that a D meson is produced from the heavy quark q, $\mathcal{B}_D$ is the branching ratio for the decay channel considered, and $\epsilon^{q \to D}$ is the identification efficiency. After background subtraction, the number of single-tagged hemispheres and double-tagged events, respectively N_s and N_d, are

$$\begin{aligned} N_s &= 2N_H(R_c\xi_c + R_b\xi_b) , \\ N_d &= N_H[R_c\xi_c^2(1+\rho) + R_b\xi_b^2\kappa_{mix}] , \end{aligned} \tag{1}$$

where N_H is the number of hadronic events, ρ accounts for a correlation in tagging efficiency between the hemispheres in charm events, and κ_{mix} is a correction for the mixing in b events. This correction is needed because in double-tagged events opposite charge c quarks are searched for. In the above formula the effect of the gluon splitting $g \to q\bar{q}$ and the correlation ρ_b in b events are neglected, nevertheless they are taken into account in the final result.

The D candidates are required to have high momentum in order to reject charmed mesons produced in b hadron decays. In both analyses the charm fraction in the single-tagged sample,

$$f_c = \frac{R_c\,\xi_c}{R_c\,\xi_c + R_b\xi_b} ,$$

is directly measured from the data using the lifetime tag. This enables the b hemisphere tagging efficiency, ξ_b, to be eliminated from Eq. 1, which becomes

$$\begin{aligned} N_s &= 2N_H R_c\xi_c/f_c , \\ N_d &= N_H R_c\xi_c^2\,[1 + \rho + \kappa_{mix}R_c(1-f_c)^2/(R_b f_c^2)] . \end{aligned} \tag{2}$$

The two equations are then solved for R_c and the tagging efficiency ξ_c.

In the first analysis both the single and double tagging require the reconstruction of high energy D mesons (D^{*+}, D^0 or D^+). In the double-tag the D meson candidates are required to have opposite charm quark charge. The second analysis uses instead a mixed double-tagging where, opposite to a reconstructed D^{*+}, a D^{*-} is identified by inclusively searching for a slow π^-. The above equations are then slightly modified as described in section 4.2.

The method where both charm quarks are tagged by an exclusive reconstruction of two D mesons has a very low background but is limited by signal statistics. Using

one inclusive tagging increases the number of double-tagged events but the statistical uncertainty is dominated by background fluctuations. As a consequence the two methods are almost completely statistically uncorrelated.

The charm fraction is measured by applying, opposite to the reconstructed D mesons, a lifetime-mass tagging [16] designed to select b hemispheres with 99% purity. The charm fraction is deduced from

$$N_s^{\text{b-tag}} = N_s \left[f_c \epsilon_{c\bar{c}} + (1 - f_c) \epsilon_{b\bar{b}} \right] \tag{3}$$

where $N_s^{\text{b-tag}}$ is the number of single-tagged events that survive the b-tagging cut, and $\epsilon_{b\bar{b}}$ and $\epsilon_{c\bar{c}}$ are the b-tagging efficiencies respectively for b and charm hemispheres.

The correlation ρ is taken from Monte Carlo simulation. Two main sources contribute to the correlation. The first is the detector acceptance, which depends on the angle of the D meson with respect to the beam axis. Since the two charm quarks are emitted nearly back-to-back, when a D meson is tagged in one hemisphere, the efficiency for tagging in the opposite hemisphere is increased. The second source of correlation is related to gluon emission, which induces a positive momentum correlation between the two primary quarks [17]. The efficiency to select a D is higher if a high momentum D is selected on the opposite hemisphere.

The correction κ_{mix} takes into account neutral B meson mixing and the $b \to cW^-$, $W^- \to \bar{c}s$ decay probability. These two processes produce a D meson of "wrong" charge which is rejected in the double-tagged sample.

4.1 Double Tagging with Fully Reconstructed D Mesons

According to Eq. 2, when the same charm tagging is applied in both hemispheres, the expression for R_c is

$$R_c = \frac{f_c^2(1+\rho)}{4N_H N_d/N_s^2 - \kappa_{\text{mix}}(1-f_c)^2/R_b} , \tag{4}$$

independent of the tagging efficiencies. Three quantities must therefore be determined from the data to measure R_c: the number of reconstructed D mesons, N_s, the charm fraction f_c in the sample, and the number of double-tagged events, N_d. The numbers of tags N_s and N_d are evaluated from the invariant mass spectra of the D meson candidates while f_c is determined using the lifetime-mass tag as explained in the previous section.

In order to increase the statistics of the double-tagged sample, the tagging is performed with a D^{*+}, a D^0 or a D^+. Any combination of two of these mesons, with opposite charm quantum number, is considered a double-tagging.

The result for R_c depends on R_b through the term $\kappa_{\text{mix}}(1-f_c)^2/R_b$, which takes into account the D mesons produced in $Z \to b\bar{b}$ events. This dependence is strongly reduced by selecting a high purity sample of D mesons from $Z \to c\bar{c}$ events.

4.1.1 Selection of D Meson Candidates

The D mesons are selected in the following decay channels:

$D^{*+} \to \pi_s^+ D^0$ with $D^0 \to K^-\pi^+$, $D^0 \to K^-\pi^+\pi^0$, $D^0 \to K^-\pi^-\pi^+\pi^+$;
$D^0 \to K^-\pi^+$;
$D^+ \to K^-\pi^+\pi^+$.

The selection of the channels $\mathbf{D^{*+} \rightarrow \pi_s^+ D^0}$, with $\mathbf{D^0 \rightarrow K^-\pi^+}$ and $\mathbf{D^0 \rightarrow K^-\pi^+\pi^-\pi^+}$ follows the same lines as in Ref. [18]. In order to further reduce the combinatorial background in the four-body case the dE/dx probability for the kaon candidate to be a kaon, $\mathcal{P}_{\rm K}$, is required to be greater than the probability to be a pion, $\mathcal{P}_\pi$.

The channel $\mathbf{D^{*+} \rightarrow \pi_s^+ D^0 \rightarrow \pi_s^+ K^-\pi^+\pi^0}$ is selected in two different ways. In a first selection, the π^0 is reconstructed from combinations of two photons detected in the electromagnetic calorimeter. Reference [15] contains a detailed description of the selection. In a second selection ($\rm D^* \rightarrow \pi_s D^0 \rightarrow \pi_s K\pi(\pi^0)$), the π^0 is not used in the $\rm D^0$ reconstruction. This recovers the $\rm D^0$'s where the π^0 is of too low momentum to be reconstructed. The selection is described in detail in Ref. [18]. Candidates common to both selections are counted once.

The $\mathbf{D^0 \rightarrow K^-\pi^+}$ sample is obtained from the pairing of two charged tracks. The kaon candidate is required to have a momentum greater than 3 GeV/c and the pion greater than 2.5 GeV/c. The mass window to select the $\rm D^0$ candidate is restricted to $1.841 < M_{\rm D^0} < 1.889$ GeV/c^2. The tracks associated to the $\rm D^0$ must come from a common vertex. The vertex position is used to reconstruct the $\rm D^0$ proper time $t_{\rm D^0}$. This $\rm D^0$ proper time and, when available, the ionization measurement for the kaon track, are used to reject the background by keeping candidates with $t_{\rm D^0} > 0.05$ ps and $\mathcal{P}_{\rm K} > \mathcal{P}_\pi$. $\rm D^0$ candidates originating from a $\rm D^{*+}$ are rejected by adding a π^+ track to the $\rm D^0$ system and removing combinations with $\Delta M = M_{\rm D^*} - M_{\rm D^0} < 0.15$ GeV/c^2.

For the $\mathbf{D^+ \rightarrow K^-\pi^+\pi^+}$ mode, a combination of three charged tracks is examined, with pion mass assignments for the two tracks with the same sign and a kaon mass assignment for the remaining track. The kaon must have a momentum greater than 3.5 GeV/c and one pion must have a momentum greater than 1.5 GeV/c. The invariant mass of the system is required to be within 30 MeV/c^2 of the $\rm D^+$ mass, corresponding to approximately twice the invariant mass resolution. $\rm D^+$ candidates consistent with the decay $\rm D^{*+} \rightarrow \pi_s^+ D^0 \rightarrow \pi_s^+ K^-\pi^+ X$ (X being mainly a π^0) are removed by a cut $\Delta M \equiv M_{K\pi\pi} - \max[M(K\pi_1), M(K\pi_2)] > 0.15$ GeV/c^2, where $M(\rm K\pi_1)$ and $M(\rm K\pi_2)$ are the invariant masses of the two Kπ combinations. All combinations are retained for which the three tracks originate at a common vertex, the reconstructed $\rm D^+$ proper time is greater than 0.2 ps and the dE/dx measurement for the kaon candidate satisfies $\mathcal{P}_{\rm K} > \mathcal{P}_\pi$.

In order to enrich the sample in D mesons originating from $\rm Z \rightarrow c\bar{c}$, the D fractional energy $X_E({\rm D}) \equiv E_{\rm D}/E_{\rm beam}$ is required to be greater than 0.5 except for the channel $\rm D^* \rightarrow \pi_s D^0 \rightarrow \pi_s K\pi(\pi^0)$, for which the X_E cut is lowered to 0.42 to take into account the missing π^0. The $\rm b \rightarrow DX$ contribution is further reduced by requiring that each track in the D hemisphere, except D decay products, be consistent with originating from the primary vertex with a probability greater than 5%.

For each event, only one candidate of a given charm quark charge is kept per hemisphere. Multiple candidates ('same-sign' D candidates in the same hemisphere) are resolved by selecting the $\rm D^0$ candidate with the mass closest to the $\rm D^0$ mass for the $\rm D^{*+}$ channels and by selecting the candidate with the largest decay length for the $\rm D^0$ and $\rm D^+$ channels. The remaining combinatorial background contributions are estimated as in [18], the background shapes being taken from Monte Carlo simulation. The final invariant mass spectrum for each channel is shown in Fig. 3. This selection leads to a single-tag sample of $N_s = 30029 \pm 239 \pm 83$ D mesons, where the first error is statistical and the second is systematic coming from the background estimation.

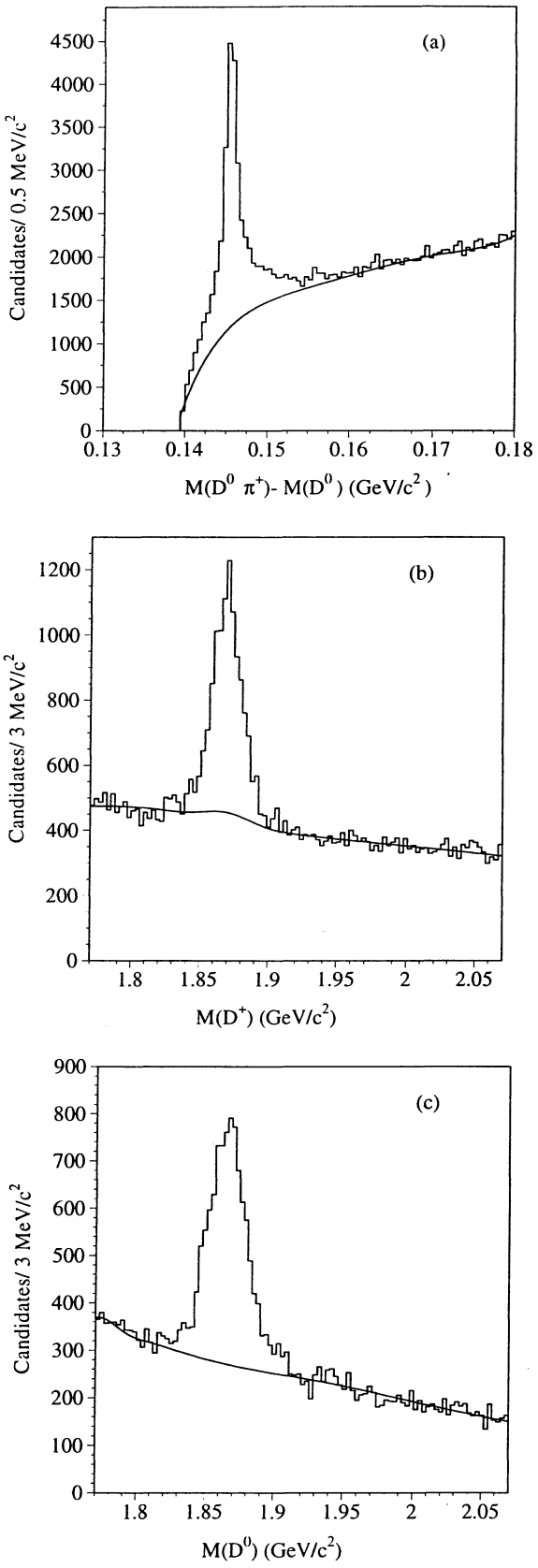

Figure 3: *Measured invariant mass distributions: (a)* $D^* \to \pi_s D^0$ *channels; (b)* $D^+ \to K\pi\pi$ *channel; (c)* $D^0 \to K\pi$ *channel. The solid line represents the background, estimated from the Monte Carlo simulation.*

4.1.2 Estimate of the Charm Fraction

The charm fraction in the single-tag sample is determined from the data according to Eq. 3, by means of a b tag [16] applied to the hemisphere opposite to the D meson candidate. Events outside the VDET acceptance are removed by requiring $|\cos\theta_{\rm thrust}| < 0.7$. A correction factor, estimated from Monte Carlo, is applied to extrapolate $f_{\rm c}$ to the whole acceptance. The requirement of a high-energy D meson in the first hemisphere reduces the fraction of events with hard gluon radiation in the sample, which in turn increases the tagging probability in the opposite hemisphere. To allow for this the tagging efficiencies are modified by a correction γ calculated from Monte Carlo:

$$\begin{array}{ll} \epsilon_{\rm c\bar{c}} = \epsilon^0_{\rm c\bar{c}}(1+\gamma_{\rm c\bar{c}}) & \epsilon_{\rm b\bar{b}} = \epsilon^0_{\rm b\bar{b}}(1+\gamma_{\rm b\bar{b}}) \\ \epsilon^0_{\rm c\bar{c}} = 0.00436 \pm 0.00031 & \epsilon^0_{\rm b\bar{b}} = 0.2271 \pm 0.0016 \\ \gamma_{\rm c\bar{c}} = 0.00 \pm 0.09 & \gamma_{\rm b\bar{b}} = 0.051 \pm 0.018_{stat} \pm 0.019_{model} \end{array}$$

The b-tag efficiency $\epsilon^0_{\rm b\bar{b}}$ on $Z \to b\bar{b}$ events is taken from data while the efficiency $\epsilon^0_{\rm c\bar{c}}$ on $Z \to c\bar{c}$ events is obtained from a Monte Carlo simulation [16]. The uncertainties on the correction factors come from the limited Monte Carlo statistics and from the uncertainties in the simulation of gluon emission. The last uncertainty is assessed by studying, in data and simulation, the momentum $p_{\rm JET}$ of the most energetic jet in a hemisphere, a quantity sensitive to the gluon radiation. As shown in Fig. 4(a) for simulated $b\bar{b}$ events, the $p_{\rm JET}$ mean value is higher when a $D^{*\pm}$ is reconstructed in the opposite hemisphere. Together with the dependence of the b tag efficiency on the $p_{\rm JET}$ value (Fig. 4(b)), this difference accounts for the correlation. Figures 4(c) and (d) compare the data and the Monte Carlo simulation. The systematic uncertainties on the correlation are estimated by weighting the b tag efficiency for the ratio between data and Monte Carlo distributions. The overall charm fraction in the single-tag sample is then found to be $f_{\rm c} = 0.890 \pm 0.015(\text{stat.}) \pm 0.005(\text{syst.})$

4.1.3 The Double-tag Sample

Within the single-tag sample, pairs of candidates from the same event are searched for. These double-tag events are retained if the two D meson candidates have opposite charm quark charge and are in opposite hemispheres. The resulting D^{*+}, D^+ and D^0 invariant mass spectra are shown in Fig. 5, with 428 candidates in the mass windows.

In addition to the signal containing two genuine D mesons, two other kind of events populate the double-tag sample. The first contribution [D-fake] comes from events where a random combination faking a D is associated with a genuine D in the other hemisphere. A smaller contribution [fake-fake] consists of events where two fake D's are selected. In order to estimate the size of these contributions, a pure combinatorial background single-tag sample is built by selecting candidates in sideband regions of the invariant mass spectra. The search for a second D meson is then repeated in these events, giving the numbers of [D-fake] and [fake-fake] candidates, after normalizing the selected sample to the expected background in the signal mass windows. The number of events with a D meson in both hemispheres is then found to be $N_d = 296.3 \pm 20.7 \pm 12.0$. The second error is systematic, due to the uncertainty on the background estimation.

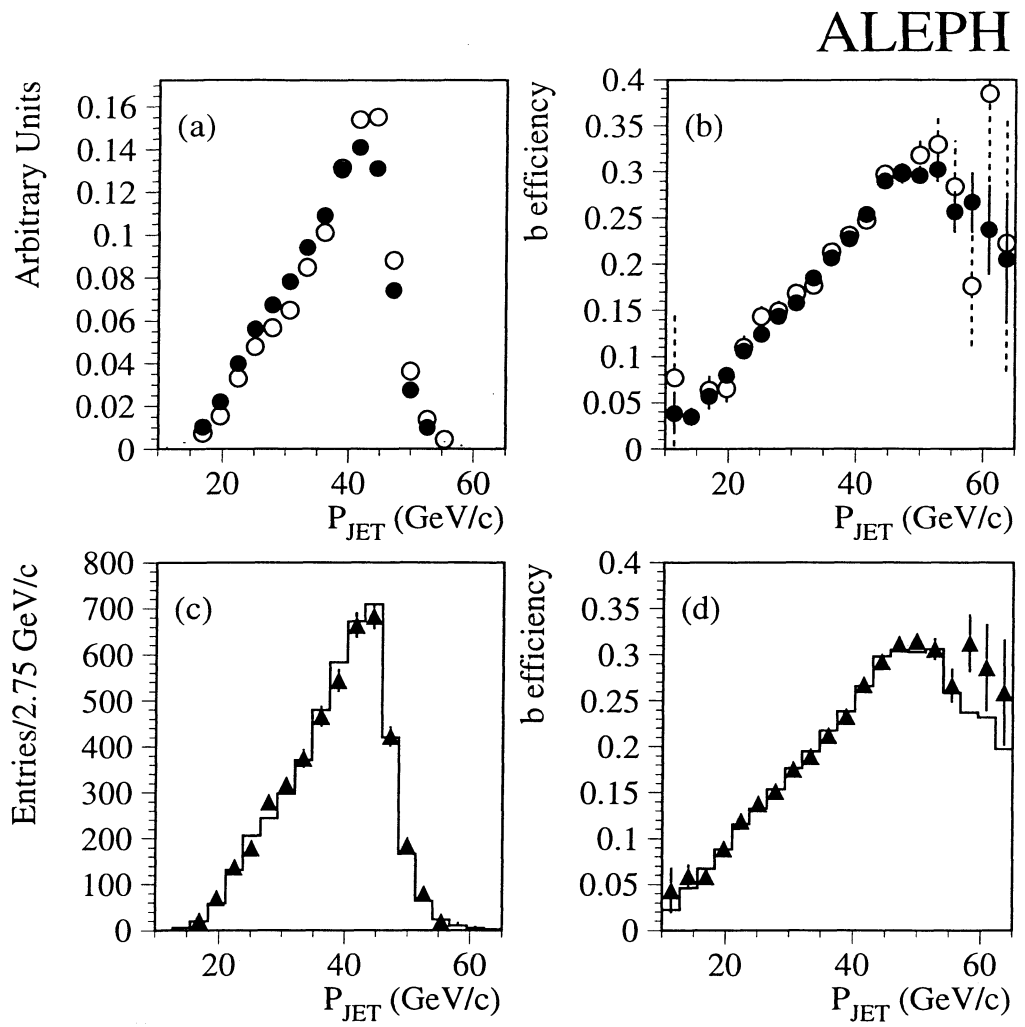

Figure 4: *The momentum* p_{JET} *of the most energetic jet (a) and the* b*-tagging efficiency in bins of* p_{JET} *(b) in a* $\mathrm{b\bar{b}}$ *Monte Carlo sample. The black dots represent the inclusive sample and the white dots the hemispheres opposite to reconstructed* $\mathrm{D}^{*\pm}$*'s. (c) and (d) compare the data (points with errors bars) and the Monte Carlo simulation (full histogram). In (c) the momentum of the most energetic jet in the hemisphere opposite to a reconstructed* $\mathrm{D}^{*+} \to \mathrm{D}^0\pi_s^+$, $\mathrm{D}^0 \to \mathrm{K}^-\pi^+$ *decay is used for the data. The background is subtracted using the distributions in the sidebands. The fraction of* $\mathrm{c\bar{c}}$ *and* $\mathrm{b\bar{b}}$ *events in the Monte Carlo simulation is fixed to the measured value. In (d) the data sample is 99% enriched in* b *content by applying the* b*-tag on the opposite hemisphere and the Monte Carlo is a pure* $\mathrm{b\bar{b}}$ *sample.*

4.1.4 Determination of R_c

The two D mesons in the double-tag events are correlated in momentum and direction, leading to a correlation in tagging efficiency. According to Monte Carlo simulation, the overall correlation term ρ (Eq 4) has the value $\rho = 0.180 \pm 0.024$, where the quoted error arises from the limited number of Monte Carlo events with two D mesons decaying in the channels studied. Systematic errors arise from the uncertainty in the Monte Carlo

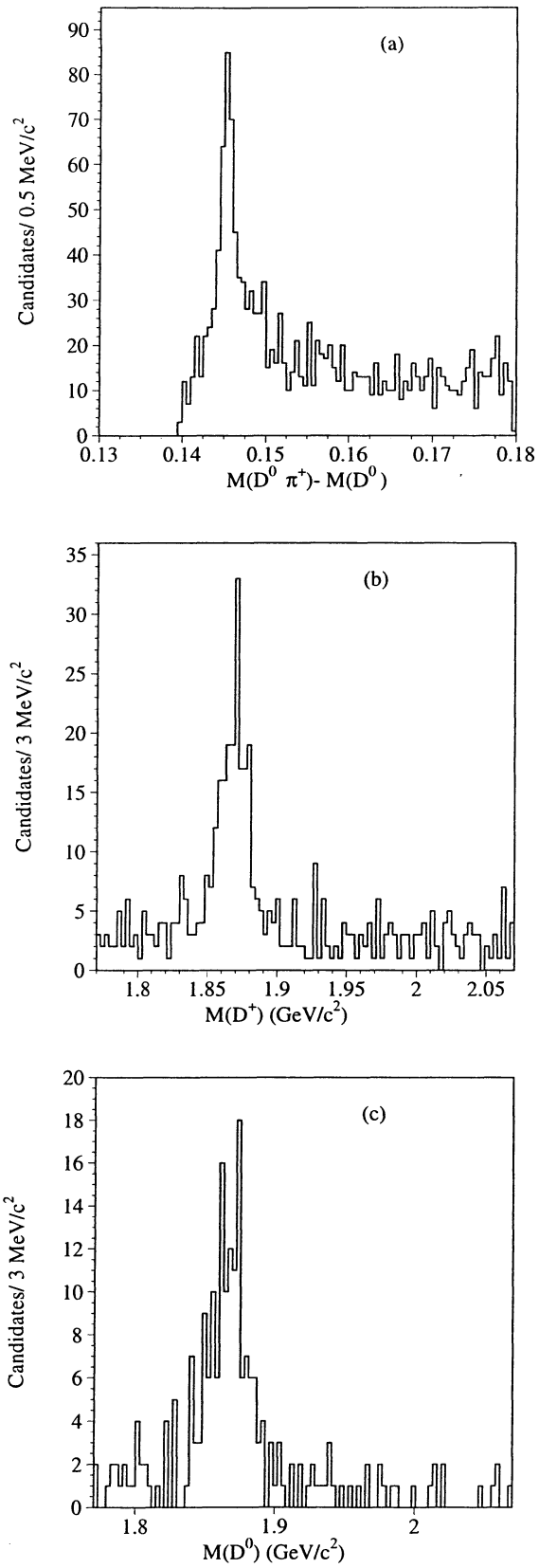

Figure 5: *Double-tag sample. Measured invariant mass distribution in opposite hemisphere after a* D *tag in the first hemisphere: (a)* $D^* \to \pi_s D^0$ *channels; (b)* $D^+ \to K\pi\pi$ *channel; (c)* $D^0 \to K\pi$ *channel.*

description of gluon emission and in the acceptance of the D mesons. Those are the two main causes of the correlation. A comparison between data and simulation is performed using variables sensitive to these two sources: the momentum of the most energetic jet in each hemisphere for the gluon radiation, and the direction of the thrust axis for the acceptance correlation. The Monte Carlo events are re-weighted to reproduce the distributions of these variables in the data. The statistical uncertainties on these corrections lead to a systematic error on ρ of 0.011. The term accounting for the correlation in double-tagged $Z \to b\bar{b}$ events is fixed to the same value as ρ with an uncertainty of 100%.

A small fraction of the D mesons originate from gluon splitting, where, in the process $Z \to q\bar{q}g$, the gluon produces two heavy quarks. In the single-tag sample this fraction is determined to be $f_g = 0.0066 \pm 0.0026$, using the measurement of the multiplicity of charm quark pairs from gluons in hadronic Z decays, $\bar{n}_{g\to c\bar{c}} = (2.27 \pm 0.50)\%$ [19], the theoretical prediction $\bar{n}_{g\to b\bar{b}} / \left(\bar{n}_{g\to b\bar{b}} + \bar{n}_{g\to c\bar{c}}\right) = 0.13 \pm 0.05$ [20], and the ratio $\xi_{g\to D}/\xi_{q\to D} = 0.049 \pm 0.016$ of the selection efficiencies for D mesons from gluon splitting and primary quarks. The number of single-tagged hemispheres, corrected for this contribution, is reduced to $N_s = 29818 \pm 237 \pm 113$. No events containing a D meson from gluon splitting are expected in the double-tag sample.

The probability to produce a "wrong" charm quark charge $\bar{D}^0$, D^- or D^{*-} meson in a b decay is found to be $\chi_D = 0.139 \pm 0.035$, calculated as in Ref. [18], using the most recent available measurements for the branching ratios of B decays into D mesons [21]. The number of double-tagged $b\bar{b}$ events with opposite charm flavour D mesons is then reduced by the factor $\kappa_{mix} = 1 - 2\chi_D(1 - \chi_D) = 0.76 \pm 0.04$.

From Eq. 4 and the measurement of N_s, N_d and f_c, one obtains

$$R_c = 0.173 \pm 0.014(\text{stat.}) \pm 0.009(\text{syst.}),$$

where the various contributions to the statistical and systematic uncertainties are listed in Table 2.

Table 2: *Contributions to the statistical and systematic uncertainties on* R_c.

Source	Stat.	Syst.
N_s	± 0.0027	± 0.0009
N_d	$^{-0.0131}_{+0.0114}$	∓ 0.0071
f_c	± 0.0053	± 0.0019
ρ	-	± 0.0040
gluon splitting	-	∓ 0.0010
κ_{mix}	-	± 0.0001
TOTAL	± 0.014	± 0.009

4.2 The D^*-π_s Double Tagging Method

In this measurement a mixed double-tagging technique is used. Once a D^{*+} is fully reconstructed, a slow pion is searched for in the opposite hemisphere. Both the numbers

of reconstructed D^{*+}'s and slow pions are then needed to extract R_c. The yields of single-tagged hemispheres and double-tagged events are

$$\begin{array}{lll} \text{single-tag } D^* & N_{D^*} = 2N_H(R_c\xi_c^{D^*} + R_b\xi_b^{D^*}) , \\ \text{single-tag } \pi_s & N_\pi = 2N_H(R_c\xi_c^{\pi} + R_b\xi_b^{\pi}) , \\ \text{double-tag} & N_d = 2N_H\left[R_c\xi_c^{D^*}\xi_c^{\pi}(1+\rho) + R_b\xi_b^{D^*}\xi_b^{\pi}\kappa'_{mix}\right] , \end{array}$$

where in N_d a factor $2N_H$, instead of N_H as in Eq. 1, arises because of the different tags applied in the two hemispheres. The tagging efficiencies, $\xi_q^{D^*}$ and ξ_q^{π} respectively for the exclusive and inclusive tag, are given by:

$$\begin{aligned} \xi_q^{D^*} &= P(q \to D^*)\mathcal{B}(D^{*+} \to D^0\pi_s^+)\mathcal{B}_{D^0}\epsilon^{q\to D^*} , \\ \xi_q^{\pi} &= P(q \to D^*)\mathcal{B}(D^{*+} \to D^0\pi_s^+)\epsilon^{q\to \pi} , \end{aligned}$$

where $\mathcal{B}_{D^0}$ is the decay ratio of the D^0 in the reconstructed channels.
As before the ξ_b tagging efficiencies are expressed in terms of the charm fractions $f_c^{D^*}$ and f_c^{π} in the single-tag samples.

The yield of slow pions, N_π, has been determined in a previous paper [11] devoted to the measurement of the branching ratio $\mathcal{B}(D^0 \to K^-\pi^+)$. However the question of whether a D^{*+} is produced in a $c\bar{c}$ or in a $b\bar{b}$ event was not addressed there. One can take advantage of the previous measurement by replacing N_π and f_c^{π} by the number of fully reconstructed $D^{*+} \to D^0\pi_s^+$, $D^0 \to K^-\pi^+$ decays, $N_{D^*}^{K\pi}$, and the charm fraction therein, $f_c^{K\pi}$, i.e.

$$\begin{aligned} f_c^{\pi}N_\pi &= \frac{f_c^{K\pi}N_{D^*}^{K\pi}}{\mathcal{B}(D^0 \to K^-\pi^+)}\frac{\epsilon^{c\to\pi}}{\epsilon^{c\to K\pi}} , \\ (1-f_c^{\pi})N_\pi &= \frac{(1-f_c^{K\pi})N_{D^*}^{K\pi}}{\mathcal{B}(D^0 \to K^-\pi^+)}\frac{\epsilon^{b\to\pi}}{\epsilon^{b\to K\pi}} , \end{aligned}$$

for the charm and beauty component, respectively. The efficiency to reconstruct the exclusive decay chain is $\epsilon^{c\to K\pi}$ ($\epsilon^{b\to K\pi}$) for the charm (beauty) component. As the branching ratio of $D^0 \to K^-\pi^+$ has been measured in [11] by comparing the yield of soft pions to the yield of the fully exclusive chain, a partial cancellation of errors between the $\mathcal{B}(D^0 \to K^-\pi^+)$ and the efficiencies of both the exclusive and the inclusive selections occurs.

The final expression for R_c is

$$\begin{aligned} R_c &= \frac{f_c^{K\pi}f_c^{D^*}(1+\rho)\epsilon^{c\to\pi}/\epsilon^{c\to K\pi}}{2N_H\mathcal{B}(D^0 \to K^-\pi^+)N_d/(N_{D^*}N_{D^*}^{K\pi}) - \delta_b} ; \\ \delta_b &= \kappa'_{mix}(1-f_c^{D^*})(1-f_c^{K\pi})\epsilon^{b\to\pi}/(R_b\epsilon^{b\to K\pi}) . \end{aligned} \tag{5}$$

The number of double-tagged events, N_d, is determined from the excess at low values in the $p_\perp^2$ distribution of slow pions with charge opposite to that of the reconstructed D^*'s. In order to subtract the background from fake π_s's and the random coincidences between true π_s's and fake D^*'s, the second tag is also applied to the pions with the same charge as the tagged D^*'s and the distribution obtained is subtracted from the opposite charge one. Therefore the events $Z \to b\bar{b}$ where a mixing occurred are thereby subtracted twice, leading to a correction factor $\kappa'_{mix} = 1 - 4\chi_D(1-\chi_D)$.

4.2.1 D^{*+} Exclusive Sample

The reconstruction of D^{*+} mesons is similar to the one already described in Sec. 4.1.1. No cut is applied here on $X_E(D^*)$. Instead the slow pion momentum is required to be greater than 1.5 GeV/c and less than 3.5 GeV/c in all channels. The same cut is applied in the inclusive selection, leading to a cancellation of the corresponding efficiency in the final expression for R_c (Eq. 5).

The number of selected D^*'s is $N_{D^*}^{K\pi} = 4439 \pm 71 \pm 53$ for the channel $D^0 \to K\pi$ only and $N_{D^*} = 25007 \pm 195 \pm 500$ for the whole sample, where the first errors are statistical and the second are systematic due to the background subtraction.

The charm fraction is determined in each channel by means of the b tag, as described in section 4.1.2, yielding $f_c^{K\pi} = 0.741 \pm 0.019(\text{stat}) \pm 0.007(\text{syst})$ in the $D^0 \to K^-\pi^+$ channel only, and $f_c^{D^*} = 0.7626 \pm 0.0094(\text{stat}) \pm 0.0066(\text{syst})$ in the whole sample. The systematic errors arise from the uncertainties on the b-tag efficiencies for b and c events. As explained in Sec. 4.1.2, these uncertainties are mainly due to the correlations between the hemisphere where the $D^{*\pm}$ has been reconstructed and the opposite one, where the b tag is applied. Corrections $\gamma_{b\bar{b}} = 0.063 \pm 0.024$ and $\gamma_{c\bar{c}} = 0.04 \pm 0.08$ are estimated from a Monte Carlo sample where the above selection cuts are applied. The errors on these are assessed as in Sec. 4.1.2, by comparing Monte Carlo and data jet momentum distributions.

4.2.2 Double-tagged Events

In the above sample the rate of $D^{*-} \to \bar{D}^0\pi_s^-$ in the hemispheres opposite to the reconstructed D^{*+}'s is measured from the excess of pions at low transverse momentum with respect to the nearest jet. A detailed discussion of the pion selection and jet axis definition is given in [11]. The π_s momentum is here required to be between 1.5 GeV/c and 3.5 GeV/c.

In Fig. 6(a) the $p_\perp^2$ distributions of the selected tracks with the opposite and the same charge with respect to the reconstructed D^* are shown. The number of double-tagged events, N_d, is extracted from a fit to the difference of the two distributions, shown in Fig. 6(b).

The shape of the $p_\perp^2$ distribution for the signal is taken from the Monte Carlo. Corrections are applied to take into account the differences between the real and simulated distributions of the D^* angle with respect to the jet and the decay angle of the pion in the D^* rest frame [11]. The long tail in the $p_\perp^2$ region above 0.05 GeV/c^2 is mainly due to tracks coming from decays of c and b hadrons other than the D^*, where the high Q value of the decay results in a broader distribution in $p_\perp^2$. The shape of these contributions is taken from Monte Carlo and the rates fixed to the latest measurements of c and b hadron production [21]. A linear component is added to the fit to take into account a net charge correlation in the tracks from fragmentation.

The fitted number of double tag events is $N_d = 1714 \pm 90 \pm 34$, where the first error is statistical and the second systematic. The systematic error coming from the signal $p_\perp^2$ shape is estimated by varying within their uncertainties the c and b contributions to the signal and the corrections applied to the shape from the Monte Carlo simulation. The systematic error due to fake π_s's is estimated by varying the contribution from b and c hadron decays by $\pm 50\%$, resulting in a 1% error. Moreover, a 1% uncertainty is added in quadrature to take into account the charge correlation between true π_s and fake D^*'s, which is estimated from a Monte Carlo simulation to be $(0.9 \pm 1.0)\%$.

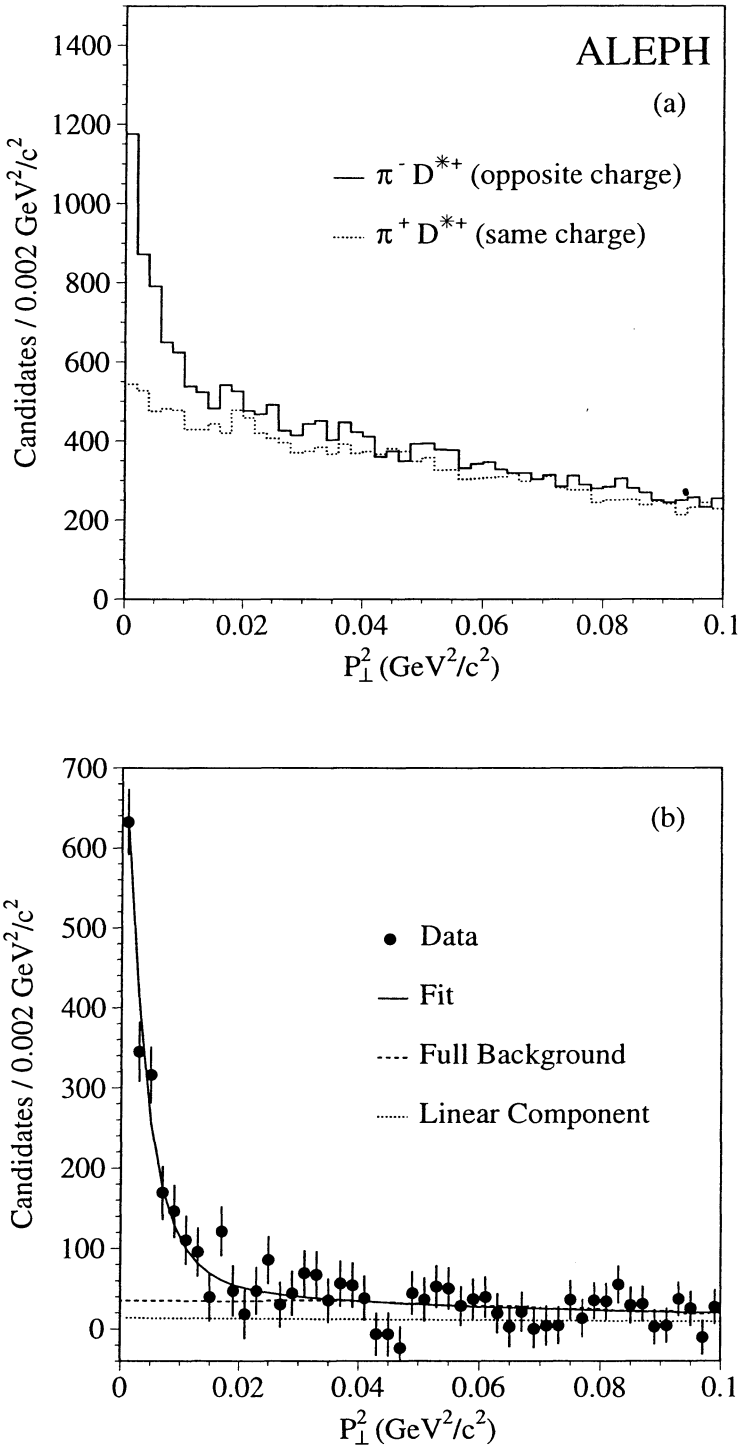

Figure 6: *Distributions of pion $p_\perp^2$ with respect to the nearest jet in double tag events. In (a) are shown the two distribution for pions with opposite charge and same charge with respect to the* D* *one. In (b) is shown the difference between the two distributions. The superimposed function is the best fit to the signal. The background is shown by the dashed line. The dotted line is the linear component of the background.*

4.2.3 Determination of R_c

The value of R_c is extracted by means of Eq. 5 from the measured numbers of single and double tags, the charm fractions in the exclusive samples, the ratio $\epsilon^{q\to\pi}/\epsilon^{q\to K\pi}$, the correlation ρ and the branching ratio $\mathcal{B}(D^0\to K^-\pi^+)$.

The efficiencies in both the exclusive and inclusive channel can be factorised with a term ϵ^{p_π} which accounts for the soft pion momentum cut and a term which account for the reconstruction efficiency ϵ_{rec}. Since in both cases the same cut is applied to the slow pion momentum, ϵ^{p_π} is equal for both exclusive and inclusive channels. The ratio of the slow pion to D^* reconstruction efficiencies then becomes $\epsilon^{q\to\pi}/\epsilon^{q\to K\pi} = (\epsilon^{p_\pi}\epsilon^{q\to\pi}_{rec})/(\epsilon^{p_\pi}\epsilon^{q\to K\pi}_{rec}) = \epsilon^{q\to\pi}_{rec}/\epsilon^{q\to K\pi}_{rec}$. The reconstruction efficiencies for the $D^{*+}\to D^0\pi_s^+$, $D^0\to K^-\pi^+$ channel are $\epsilon^{c\to K\pi}_{rec} = (62.5\pm0.4\pm0.9)\%$ for c events and $\epsilon^{b\to K\pi}_{rec} = (63.1\pm0.7\pm0.9)\%$ for b events. The first errors are due to the limited Monte Carlo statistics used, while the second ones are the fully correlated systematic errors coming from nuclear interactions, the mass cuts and the two-track resolution when the pion and kaon tracks overlap. The inclusive channel reconstruction efficiency was calculated in [11], where it was found to be $(72.6\pm0.2)\%$ for both c and b events. From a Monte Carlo simulation, the ρ correlations are found to be $\rho_c = 0.228\pm0.025$ and $\rho_b = 0.42\pm0.22$, with the errors calculated as explained in Section 4.1.4.

The value used for the branching ratio, $\mathcal{B}(D^0\to K^-\pi^+) = (3.90\pm0.09\pm0.12)\%$, is that obtained by ALEPH [11], using fully reconstructed $D^{*+}\to D^0\pi_s^+$, $D^0\to K^-\pi^+$ decays and the slow pion tagging to select inclusive D^*'s. The uncertainties on the signal $p_\perp^2$ shape and the efficiencies are sources of systematic error both for the $\mathcal{B}(D^0\to K^-\pi^+)$ measurement and for this R_c measurement. The effects of the uncertainties almost cancel in the calculation of R_c (Eq. 5), leading to a significant reduction in the final systematic uncertainty.

From the number of reconstructed $D^{*\pm}$'s, $N_{D^*}^{K\pi}$ and N_{D^*}, the contribution of the gluon splitting must be subtracted. From the measurements quoted in Sec. 4.1.4, a fraction $f_g = (0.9\pm0.4)\%$ of the selected $D^{*\pm}$'s is estimated to come from this source. No contribution to the double tag sample is expected from gluon splitting because of the momentum cuts on the soft pion.

The χ_D probability that a "wrong" charge D^{*-} is produced in a b decay is here $\chi_D = 0.189\pm0.032$, which leads to a mixing correction $\kappa'_{mix} = 0.39\pm0.08$.

The result obtained from Eq. 5 is

$$R_c = 0.166\pm0.012(\text{stat.})\pm0.009(\text{syst.})\ .$$

The sources of statistical and systematic error are listed in Table 3.

4.3 Combination of the two double-tagging methods

The two measurements using charmed mesons are combined, taking into account the correlated statistical and systematic errors on the number of single-tagged hemispheres, the charm fraction, the correlation, b mixing and gluon splitting (see table 4).

This yields an average value

$$R_c = 0.1689\pm0.0095(\text{stat})\pm0.0068(\text{syst})\ .$$

The dependence of the result on the R_b value is given by $R_c = 0.1689 - 0.023\times(R_b - 0.2159)$.

Table 3: *Variation of* R_c *due to statistical and systematic errors for the double tag method* D^*-π_s.

Source	Stat.	Syst.
N_{D^*}, $N_{D^*}^{K\pi}$	± 0.0029	± 0.0049
N_d	$^{-0.0086}_{+0.0095}$	∓ 0.0032
f_c	± 0.0047	± 0.0027
$\epsilon^{q\to K\pi}$	-	∓ 0.0019
$\epsilon^{q\to\pi}$	-	± 0.0006
ρ	-	± 0.0038
$\mathcal{B}(D^0\to K^-\pi^+)$	∓ 0.0041	∓ 0.0030
gluon splitting	-	∓ 0.0014
κ'_{mix}	-	± 0.0012
TOTAL	± 0.012	± 0.009

Table 4: *Correlated and uncorrelated errors for the combination of the double-tagging methods.*

Uncorr. Stat.	± 0.0087
Corr. Stat.	± 0.0038
TOTAL Stat.	± 0.0095
Uncorr. Syst.	± 0.0050
charm fraction	
b-tag efficiencies DATA stat.	∓ 0.0004
b-tag efficiencies MC stat.	∓ 0.0002
b-tag efficiencies b-physics	∓ 0.0001
b-tag efficiencies udsc-physics	∓ 0.0004
b-tag efficiencies tracking	∓ 0.0002
b-tag efficiencies MC modeling	∓ 0.0001
b-tag correlations MC stat	∓ 0.0012
b-tag correlations MC modeling	∓ 0.0016
D-D correlations	
c-tag correlations MC stat	± 0.0031
c-tag correlations MC modeling	± 0.0019
c-tag correlations $< X_E >= 0.495 \pm 0.013$ [15]	± 0.0012
B meson mixing	
$\chi_d = 0.175 \pm 0.016$ [21]	∓ 0.0003
$b \to D\bar{D}X = 0.03 \pm 0.03$ [18, 21]	∓ 0.0006
gluon splitting	
$\bar{n}_{g\to c\bar{c}} = (2.27 \pm 0.50)\%$ [19]	∓ 0.0006
$\bar{n}_{g\to b\bar{b}} / \left(\bar{n}_{g\to b\bar{b}} + \bar{n}_{g\to c\bar{c}}\right) = 0.132 \pm 0.047$ [20]	∓ 0.0001
$\xi_{g\to D}/\xi_{q\to D}$	∓ 0.0010
TOTAL Syst.	± 0.068

5 Conclusion

Three measurements of the partial decay width of the Z into $c\bar{c}$ quarks have been performed. The first one uses inclusive electrons and takes advantage of an accurate knowledge of the b and non-prompt components of the electron yield. A fit to the p and $p_\perp$ electron spectra gives $R_c = 0.1675 \pm 0.0062(\text{stat}) \pm 0.0066(\text{syst}) \pm 0.0084(\text{BR})$.

Two other measurements, which use charmed meson decays as a charm quark signature, lead to a combined result of $R_c = 0.1689 \pm 0.0095(\text{stat}) \pm 0.0068(\text{syst})$.

The combination of these three measurements and a previous one, obtained with leptons by ALEPH from data collected in 1990 and 1991 [14], gives the following average:

$$R_c = 0.1681 \pm 0.0054(\text{stat}) \pm 0.0062(\text{syst}),$$

in agreement with the Standard Model prediction of $R_c = 0.1723$. This result is weakly correlated with the R_b value, the dependence being $R_c = 0.1681 - 0.011 \times (R_b - 0.2159)$. With the present 0.5% [22] relative error on R_b, this correspond to a systematic error of order 10^{-5}, which is negligible with respect to the quoted systematics.

Acknowledgements

We thank our colleagues from the accelerator divisions for the successful operation of the LEP machine and the engineers and technical staff in all our institutions for their contribution to the good performance of ALEPH. Those of us from non-member states thank CERN for its hospitality.

References

[1] P. Bamert, Int. J. Mod. Phys. **A12** (1997) 723;
K. Agashe, M. Graesser, I. Hinchliffe, and M. Suzuki, Phys. Lett. **B385**, (1996) 218, with further references therein.

[2] ALEPH Collaboration, *Update of electroweak parameters from Z decays*, Z. Phys. **C60** (1993) 71.

[3] ALEPH Collaboration, *ALEPH: A Detector for Electron - Positron Annihilations at LEP*, Nucl. Instr. Methods **A294** (1990) 121.

[4] ALEPH Collaboration, *Performance of the ALEPH detector at LEP*, Nucl. Instr. Methods **A360** (1995) 481.

[5] ALEPH Collaboration, *Heavy quark tagging with leptons in the ALEPH detector*, Nucl. Instr. Methods **A346** (1994) 461.

[6] P. Perret, *Measurement of heavy quark electroweak properties in Z decays using inclusive leptons at LEP*, Proceeding of the 1995 International Europhysics Conference on High Energy Physics, Brussels, edited by J. Lemonne *et al.*(World Scientific, New Jersey, 1996).

[7] ALEPH Collaboration, *A Precise measurement of* $\Gamma(Z \to b\bar{b})/\Gamma(Z \to hadrons)$, Phys. Lett. **B313** (1993) 535.

[8] C. Peterson *et al.*, Phys. Rev. **D27** (1983) 105.

[9] The LEP Electroweak Working Group for the LEP Experiments, *Combining Heavy Flavour Electroweak Measurements at LEP*, Nucl. Instr. Methods **A378** (1996) 101.

[10] G. Altarelli *et al.*, Nucl. Phys **B208** (1982) 365;
G. Altarelli and S. Petrarca, Phys. Lett. B261 (1991) 303.

[11] ALEPH Collaboration, *Measurement of the branching fraction for* $D^0 \to K^-\pi^+$, Phys. Lett. **B403** (1997) 367.

[12] P. Collins and T. Spiller, J. Phys. G11, (1985) 1289.

[13] V.G. Kartvelishvili, *et al.*, Phys. Lett. **B78** (1978) 615.

[14] ALEPH Collaboration, *Heavy flavour production and decay with prompt leptons in the ALEPH detector*, Z. Phys. **C62** (1994) 179.

[15] ALEPH Collaboration, *Production of charmed mesons in Z decays*, Z. Phys. **C62** (1994) 1.

[16] ALEPH Collaboration, *A Measurement of* R_b *using a lifetime mass tag*, Phys. Lett. **B401** (1997) 150; *A Measurement of* R_b *using mutually exclusive tags*, Phys. Lett. **B401** (1997) 163.

[17] P. Nason and C. Oleari, Phys. Lett. **B387** (1996) 623; Phys. Lett. **B407** (1997) 57.

[18] ALEPH Collaboration, *The Forward-Backward Asymmetry for Charm Quarks at the Z Pole*, Phys. Lett. **B352** (1995) 479.

[19] OPAL Collaboration, *Measurement of the Multiplicity of Charm Quark Pairs from Gluons in Hadronic Z^0 Decays*, Phys. Lett. **B353** (1995) 595.

[20] M.H. Seymour, Nucl. Phys **B436** (1995) 163.

[21] Particle Data Group, Phys. Rev. **D54** (1996) 1.

[22] The LEP Collaborations ALEPH, DELPHI, L3, OPAL, the LEP Electroweak Working Group and the SLD Heavy Flavour Group, *A Combination of Preliminary Electroweak Measurements and Constraints on the Standard Model*, CERN-PPE/97-154.